SUPPLEMENTARY INFORMATION

Mechanism of action of two potent LRRC8/VRAC channel inhibitors

Sara T. Granados[1], Richard Song[1], Francisca Añazco[1], Jose M. Vermejo[1], Yan Rao[1], and Axel R. Concepcion[1,2,3,4*]

[1] Department of Biochemistry & Molecular Biology, [2] Committee on Immunology, [3] Institute for Biophysical Dynamics, [4] University of Chicago Medicine Comprehensive Cancer Center, The University of Chicago, Chicago, IL, USA.

Supplementary Figure 1. Hallmark gene pathways activated and inhibited upon T cell receptor (TCR) stimulation. Enriched pathways from the Hallmark Gene Sets (1) in wild-type murine $CD4^+$ T cells before and after 24h and 48h of anti-CD3+CD28 stimulation (GSE163679) (2), and represented as normalized enrichment scores (NES). The activation of these pathways contributes to T cell proliferation, survival, and cytokine production. Statistical analysis by Benjamini-Hochberg correction for multiple testing. *p <0.05, **p <0.01, ***p <0.001.

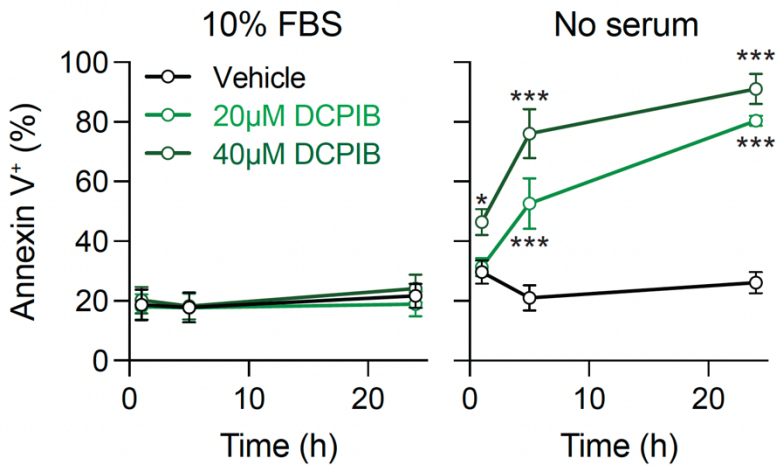

Supplementary Figure 2. DCPIB impairs the survival of Jurkat cells in serum-free conditions. Quantification of apoptosis measured by annexin V staining in Jurkat cells treated with vehicle, 20 μM, and 40 μM DCPIB in full RPMI medium with (left) and without (right) FBS at the indicated time points. Data are the mean ± SEM of *n* = 4 treatment per group, pooled from 4 independent experiments done in duplicate. Statistical analysis by a two-tailed, unpaired Student's *t*-test. **p* <0.05, ****p* <0.001.

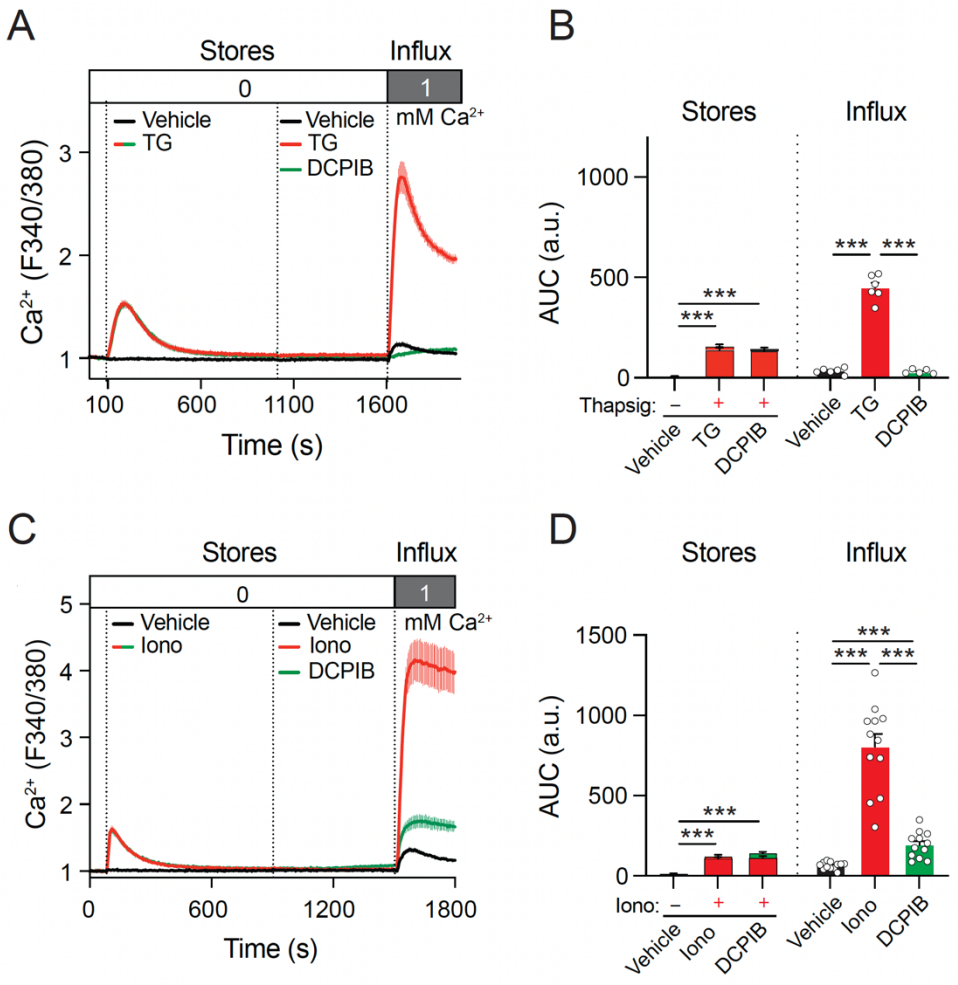

Supplementary Figure 3. DCPIB inhibits SOCE in Jurkat cells and primary human T cells. A-D Cytosolic Ca^{2+} signals in Jurkat cells (**A**, **B**) and primary human T cells (**C**, **D**). Averaged cytosolic Ca^{2+} levels (**A**, **C**) and quantification (**B**, **D**) as the area under the curve (AUC) in the region indicated by the dotted lines. Ca^{2+} signals were monitored in Fura-2-loaded T cells treated with either vehicle, 1μM thapsigargin (TG), 1μM ionomycin (Iono), or 20 μM DCPIB. Ca^{2+} signals from intracellular stores were monitored in Ca^{2+}-free Ringer's solution (ER stores: ~90-900 s, non-ER stores: ~900-1500 s), followed by re-addition of extracellular Ca^{2+} (influx: ~1500-1800 s). Ca^{2+} stores are shown as the cumulative of ER stores + non-ER stores. Data shown in (**A**-**B**) and (**C, D**) are the mean ± SEM of *n* = 6 and 12 Ca^{2+} traces, respectively, pooled from 2 and 3 independent experiments, with each group run in triplicate. Human T cells were isolated from two healthy donors. Statistical analysis by a two-tailed, unpaired Student's *t*-test. ****p* <0.001.

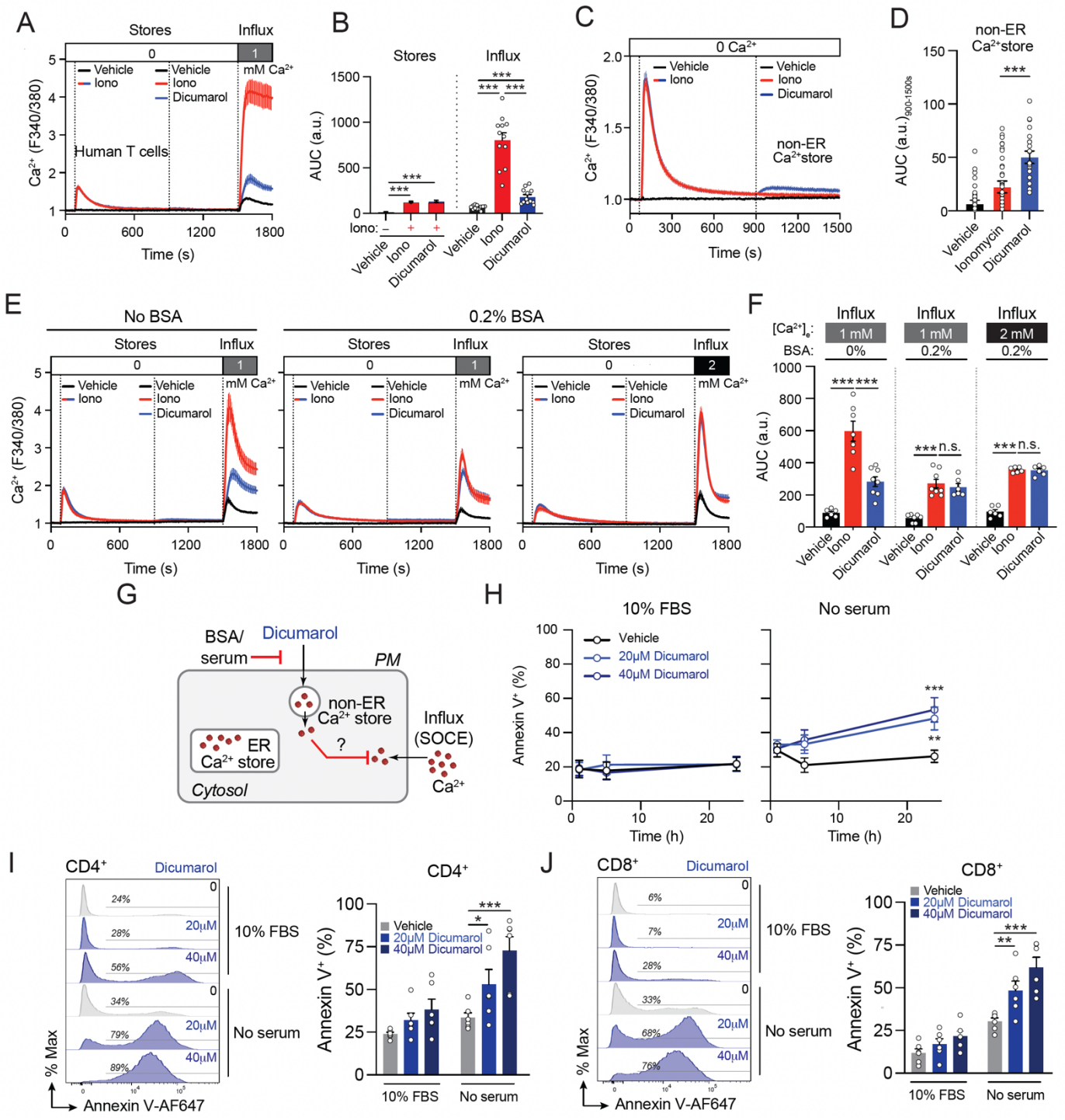

Supplementary Figure 4. Dicumarol alters intracellular Ca^{2+} signals and induces apoptosis in human and mouse T cells in albumin/serum-free conditions. A, **B** Cytosolic Ca^{2+} signals in primary human T cells. Averaged cytosolic Ca^{2+} levels (**A**) and quantification (**B**) as the area under the curve (AUC) in the region indicated by the dotted lines. Ca^{2+} signals were monitored in Fura-2-loaded human T cells treated with either vehicle, 1μM ionomycin (Iono), or 20 μM dicumarol. Ca^{2+} signals from intracellular stores were monitored in Ca^{2+}-free Ringer's solution (ER stores: 90-900 s, non-ER stores: 900-1500 s), followed by re-addition of extracellular Ca^{2+} (influx: 1500-1800 s). Ca^{2+} stores are shown as the cumulative of ER stores +

non-ER stores. **C, D** Zoom in of cytosolic Ca^{2+} stores (0-1500s) in Jurkat cells monitored in Ca^{2+}-free Ringer's solution of the experiment shown in (**Fig. 5E**). Averaged Ca^{2+} traces (**C**) and quantification (**D**) as the AUC in the non-ER Ca^{2+} stores phase upon treatment with vehicle, 1μM Iono, or 20 μM dicumarol. **E**, **F** Averaged Ca^{2+} traces (in **E**) and quantification (in **F**) of the Ca^{2+} influx response in Jurkat cells treated as in (**Fig. 5E**) in the absence and presence of 0.2% bovine serum albumin (BSA) and different concentrations of extracellular Ca^{2+} (1 mM or 2 mM). **G** Schematic model of cytosolic Ca^{2+} signals triggered by dicumarol. **H** Quantification of apoptosis measured by annexin V staining in Jurkat cells treated with vehicle, 20 μM and 40 μM dicumarol in full RPMI media with (left) and without (right) FBS at the indicated time points. **I**, **J** Apoptosis in activated murine T cells. Representative flow cytometry plots (left) and quantification (right) of apoptosis in $CD4^+$ (**I**) and $CD8^+$ (**J**) T cells measured by annexin V staining. T splenocytes were activated with anti-CD3+CD28 for 2 days, then cultured in RPMI medium with and without 10% FBS in the absence or presence of 20 μM and 40 μM dicumarol for an additional 24 h. Data shown in (**A**-**F**, **H**-**J**) are the mean ± SEM of n = 12 Ca^{2+} traces of human T cells isolated from two healthy donors, pooled from 4 independent (in **A**, **B**); n = 6-23 Ca^{2+} traces of Jurkat cells, pooled from 3 independent experiments, with each group run either in duplicate or triplicate (in **C**-**F**); n = 4 treatment per group, pooled from 4 independent experiments done in duplicate (in **H**), n = 6 mice per group, pooled from 3 independent experiments (in **I**, **J**). Statistical analysis by a two-tailed, unpaired Student's t-test and 2-way ANOVA with Dunnett's multiple comparisons (**I**, **J**). n.s. not significant, *p <0.05, **p <0.01, ***p <0.001.

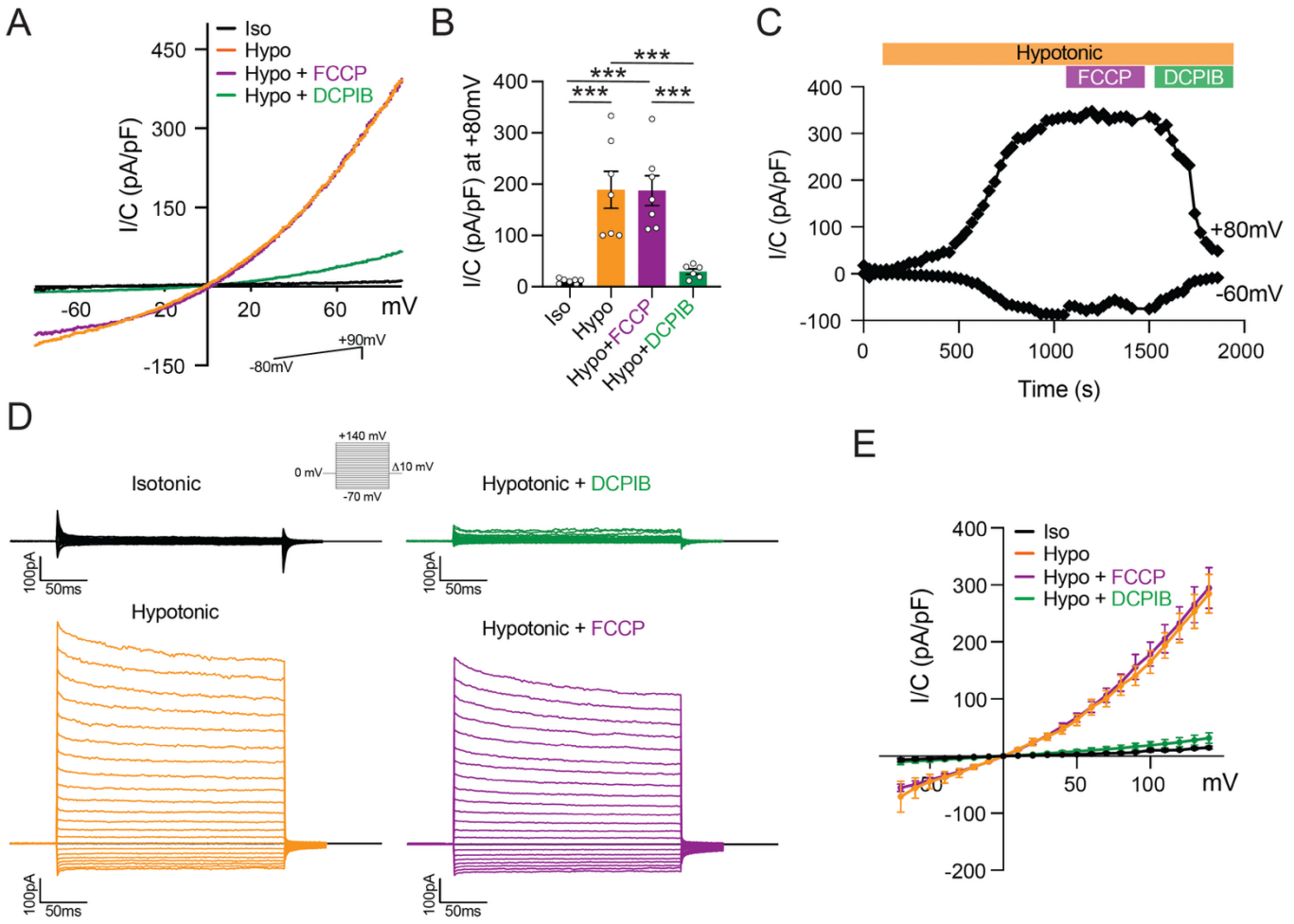

Supplementary Figure 5. DCPIB inhibits VRAC independently of its effects on mitochondrial depolarization and Ca^{2+} signaling. **A-C** Swelling-activated I_{VRAC} in Jurkat cells upon hypotonic challenge and treatment with pharmacological agents. Whole-cell currents in Jurkat cells were monitored in isotonic solution (~310 mOsm) for 2 min, followed by a perfusion of hypotonic buffer (~210 mOsm) in the bath solution for 30 min. At the 18-min mark, 1.5 μM FCCP was added to the hypotonic bath solution for an additional 7 min. After this, a wash with hypotonic buffer was performed, and 20μM DCPIB in hypotonic solution was introduced at the 25-min mark. Currents were monitored for an additional 5 min. **A** Representative current density plotted as a function of voltage monitored by a voltage ramp protocol in isotonic (Iso), hypotonic (Hypo), and after treatment with 1.5 μM FCCP or 20 μM DCPIB in hypotonic solution (Hypo+FCCP, or Hypo+DCPIB, respectively). **B** Quantification of current densities shown in (A) at +80 mV. **C** Time-response plot of current densities at +80mV and -60 mV. **D** Representative chloride current recordings from a voltage step protocol (-70 mV to +140 mV, Δ10mV). **E** Current-voltage relationship (I/V) measured at the steady state (390 ms). Data shown in (**B**) are the mean ± SEM of *n* = 6-7 cells per condition, pooled from 3 independent experiments. Statistical analysis by a two-tailed, unpaired Student's *t*-test. ***p <0.001.

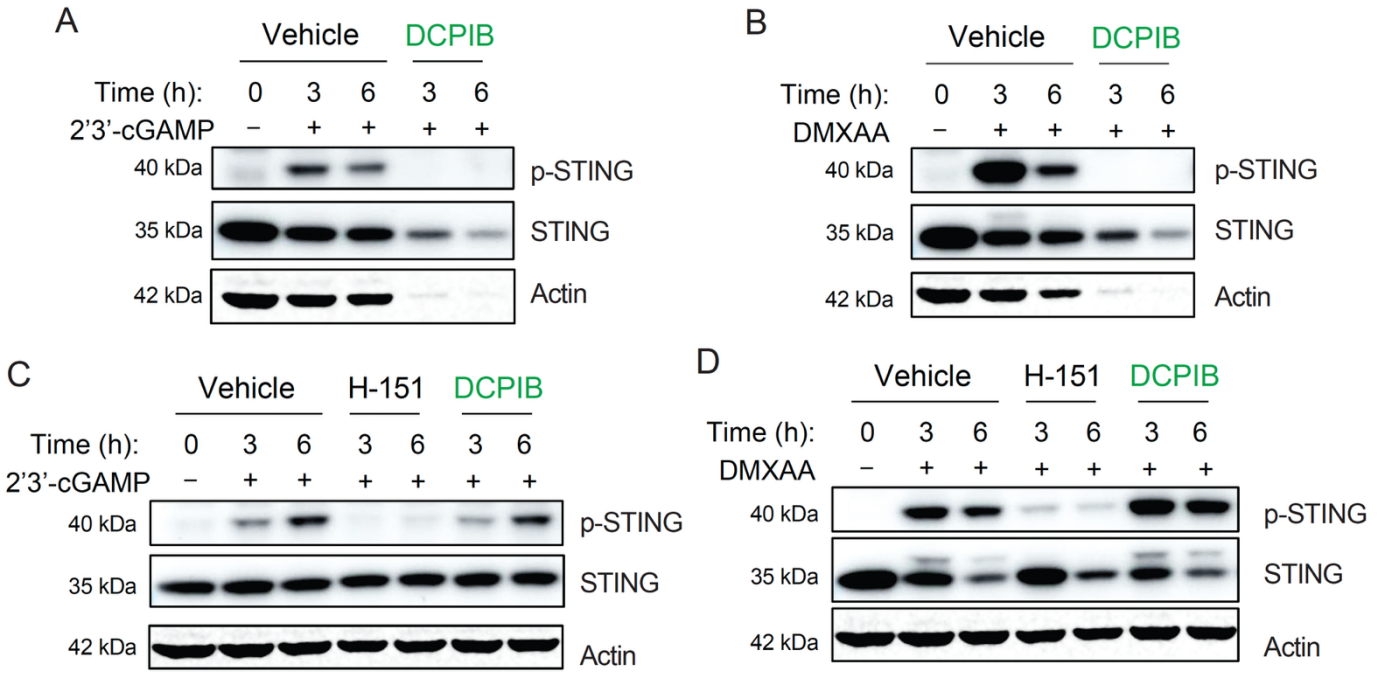

Supplementary Figure 6. DCPIB fails to suppress STING activation through inhibition of VRAC-dependent cGAMP transport in T cells under standard culture conditions. A-D Immunoblots of total and phosphorylated STING (p-STING S365) proteins in wild-type murine $CD4^+$ T cells activated for 2 days with anti-CD3+CD28. T cells were treated with vehicle (control), 20μM DCPIB, and STING agonists: 10 μg/ml 2'3'-cGAMP (in **A**) or 3 μg/ml DMXAA (in **B**) in Ringer's buffer at the indicated time points. Alternatively, in standard culture conditions (*i.e.*, full RPMI media containing 10% FBS), T cells were treated with vehicle, 10μM of STING inhibitor H-151, 20μM DCPIB, and STING agonists: 10 μg/ml 2'3'-cGAMP (in **C**) or 3 μg/ml DMXAA (in **D**) at the indicated time points. Actin was used as a loading control. Representative blots in (**A-D**) from at least 2 independent experiments.

REFERENCES

1. Liberzon A, Birger C, Thorvaldsdottir H, Ghandi M, Mesirov JP, Tamayo P. The Molecular Signatures Database (MSigDB) hallmark gene set collection. Cell Syst. 2015;1(6):417–25.

2. Concepcion AR, Wagner LE^{2nd}, Zhu J, Tao AY, Yang J, Khodadadi-Jamayran A, et al. The volume-regulated anion channel LRRC8C suppresses T cell function by regulating cyclic dinucleotide transport and STING-p53 signaling. Nat Immunol. 2022;23(2):287–302.